Archive of Applied Mechanics 66 (1996) 315–325 © Springer-Verlag 1996

Dynamic stiffness matrix of a general cable element

A. Sarkar, C. S. Manohar

Summary A computational scheme for determining the dynamic stiffness coefficients of a linear, inclined, translating and viscously/hysteretically damped cable element is outlined. Also taken into account is the coupling between inplane transverse and longitudinal forms of cable vibration. The scheme is based on conversion of the governing set of quasistatic boundary value problems into a larger equivalent set of initial value problems, which are subsequently numerically integrated in a spatial domain using marching algorithms. Numerical results which bring out the nature of the dynamic stiffness coefficients are presented. A specific example of random vibration analysis of a long span cable subjected to earthquake support motions modeled as vector gaussian random processes is also discussed. The approach presented is versatile and capable of handling many complicating effects in cable dynamics in a unified manner.

Key words dynamic stiffness, extensible cables, earthquake loads

1 Introduction

The equations governing the motion of suspended cables and their solutions have been a subject of extensive study in vibration engineering literature [2, 6, 8, 11, 13]. These studies assume their importance due to many applications of the suspended cable structures, e.g. suspension cable bridges, power transmission lines, guyed towers, conveyer systems and mooring cables, to name only a few. The study of cable dynamics becomes all the more challenging to an analyst when one considers the complicating effects of geometric nonlinearities [11], gyroscopic effects caused due to axial motion [14], coupling between different modes of vibrations [3], complexities in loading conditions such as multi-support seismic excitations [9], and material nonlinearities [13]. The present study considers the linear dynamics of a cable element including the effects of

- cable extensibility,
- coupling between longitudinal and in-plane transverse modes,
- inhomogeneities in mass, stiffness and damping properties,
- arbitrary random/deterministic loads,
- multi-support and/or multi-component time-varying boundary excitations,
- proportional/nonproportional, viscous/hysteretic damping models,
- axial motion for homogeneous cable elements and
- arbitrary chord inclinations.

The objectives of the study are twofold: firstly, we derive the dynamic stiffness matrix for the cable element taking into account the effects listed above and using the space domain numerical integration technique. Secondly, two specific examples, namely, the multi-support random seismic response of a 1000-m-long suspended cable, and the frequency response functions of an axially moving inclined cable are studied using the approach mentioned above.

Received 18 May 1995; accepted for publication 1 October 1995

A. Sarkar, C. S. Manohar
Department of Civil Engineering, Indian Institute of Science,
Bangalore 560 012, India

The work reported in this paper has been carried out as a part of a research project on dynamics of extensible cables funded by the Department of Science and Technology, Government of India. The financial support received is gratefully acknowledged.

The dynamic stiffness coefficient $\tilde{D}_{ij}(\omega)$ [7] is defined as the amplitude of a harmonic force of frequency ω applied at node i which is required to produce a unit harmonic displacement of frequency ω at node j. These complex in nature coefficients are functions of stiffness, mass and damping properties of the system and frequency of harmonic excitation. This is in contrast with the static stiffness coefficients which are functions of stiffness alone and independent of excitation characteristics. The formulation of dynamic stiffness coefficients enables the study of dynamics of built-up structures using matrix assembling techniques as used in the traditional finite element method. The determination of $\tilde{D}_{ij}(\omega)$ requires the solution of an associated quasi-static boundary value problem. For a homogeneous string, rod or beam element, exact solutions in closed form to this problem are readily available [7]. However, for a general cable element, as proposed to be studied in this paper, exact closed form solutions are not possible. In earlier studies [2], [12], and [10] approximate analytical solutions were obtained under a set of assumptions. In the present study, we convert the set of governing boundary value problems (BVPS) into a larger set of equivalent initial value problems (IVPS), and solve the resulting equations numerically using marching techniques. A distinguishing feature of this approach is that it avoids the need for carrying out a free vibration analysis, which is an inevitable first step for modal expansion methods. The solutions obtained here are exact in nature except for the round-off and truncation errors which inevitably occur in numerical solution of differential equations. It must be noted that the idea of deriving transfer functions of distributed systems by solving a set of initial value problems is not new. In a series of recent papers [4, 15, 16], the usefulness of this method in the study of beam structure dynamics is discussed. In the context of cable dynamics, however, the approach outlined in this study accounts for several complicating features of cable vibration, and is believed to be new. The wide ranging validity of approach is essentially arising from the adoption of numerical integrations in space domain.

2
Equations of motion

The first step in setting up equations of motion of a suspended cable is to determine the static deflection profile. By considering the equilibrium of an infinitesimal element of the cable shown in Fig. 1, and by assuming that the cable is inextensible, the equation governing the static profile can be shown to be given by

$$\frac{\mathrm{d}}{\mathrm{d}s}\left[T\frac{\mathrm{d}x}{\mathrm{d}s}\right]+mg\sin\theta=0,$$

$$\frac{\mathrm{d}}{\mathrm{d}s}\left[T\frac{\mathrm{d}y}{\mathrm{d}s}\right]+mg\cos\theta=0, \tag{1}$$

where m is mass per unit length, and g-acceleration due to gravity. Furthermore, under the assumption that the cable sag-to-span ratio is small, one can take $\mathrm{d}x \simeq \mathrm{d}s$. Ignoring the effect of $mg\sin\theta$ on sag, the static profile can be shown as

$$y(x)=\frac{mgL^2\cos\theta}{2H_0}\left[\left(\frac{x}{L}\right)-\left(\frac{x}{L}\right)^2\right]. \tag{2}$$

The cable tension $H(x)$ now varies along the cable, and is given by

$$H(x)=H_0+\frac{mgL}{2}\sin\theta\left[\left(\frac{2x}{L}\right)-1\right]. \tag{3}$$

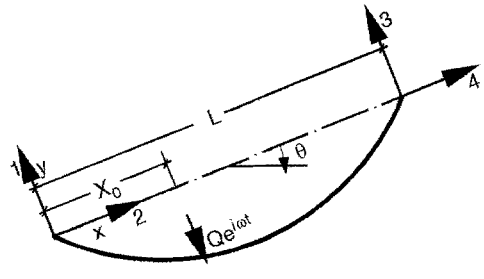

Fig. 1. Cable element

Notice that for $\theta = 0$, one gets $H(x) = H_0$. The applied horizontal tension for this case remains constant for all x.

The equation governing the dynamic displacements $v(x)$ and $u(x)$ along the transverse and chordwise directions can be derived by applying Hamilton's principle

$$\delta \int_{t_1}^{t_2} (T - U)\,\mathrm{d}t + \int_{t_1}^{t_2} \delta W_{nc}\,\mathrm{d}t = 0. \tag{4}$$

For a damped cable one gets

$$T = \frac{1}{2}\int_0^L m(x)\left\{\left[\frac{\partial v}{\partial t} + v_0\frac{\partial v}{\partial x}\right]^2 + \left[\frac{\partial u}{\partial t} + v_0\frac{\partial u}{\partial x}\right]^2\right\}\mathrm{d}x, \tag{5}$$

$$U = \int_0^L H(x)\left[\frac{\partial u}{\partial x} + \frac{\mathrm{d}y}{\mathrm{d}x}\frac{\partial v}{\partial x} + \frac{1}{2}\left(\frac{\partial u}{\partial x}\right)^2 + \frac{1}{2}\left(\frac{\partial v}{\partial x}\right)^2\right]\mathrm{d}x + \int_0^L \frac{1}{2}EA\left[\frac{\partial u}{\partial x} + \frac{\mathrm{d}y}{\mathrm{d}x}\frac{\partial v}{\partial x} + \frac{1}{2}\left(\frac{\partial u}{\partial x}\right)^2 + \frac{1}{2}\left(\frac{\partial v}{\partial x}\right)^2\right]^2\mathrm{d}x, \tag{6}$$

$$\delta W_{nc} = \int_0^L \left\{\frac{\partial^2}{\partial t\,\partial x}\left[C_1\frac{\partial u}{\partial x} + C_2\frac{\partial v}{\partial x}\right] + \frac{C_3}{\omega}\frac{\partial u}{\partial x} - C_4\frac{\partial u}{\partial t}\right\}\delta u\,\mathrm{d}x + \int_0^L \left\{\frac{\partial^2}{\partial t\,\partial x}\left[C_5\frac{\partial u}{\partial x} + C_6\frac{\partial v}{\partial x}\right] + \frac{C_7}{\omega}\frac{\partial v}{\partial x} - C_8\frac{\partial v}{\partial t}\right\}\delta v\,\mathrm{d}x. \tag{7}$$

Substituting these equations into (4) and retaining only linear terms, the governing equations for cable motion are obtained as

$$\frac{\partial}{\partial x}\left[H(x)\frac{\partial v}{\partial x} + EA(x)\frac{dy}{dx}\frac{\partial u}{\partial x} + EA(x)\left(\frac{\mathrm{d}y}{\mathrm{d}x}\right)^2\frac{\partial v}{\partial x}\right] + \frac{\partial^2}{\partial x\,\partial t}\left[C_1(x)\frac{\partial u}{\partial x} + C_2(x)\frac{\partial v}{\partial x}\right] + \frac{C_3(x)}{\omega}\frac{\partial v}{\partial t}$$
$$= \frac{\partial}{\partial t}\left[m(x)\frac{\partial v}{\partial t}\right] + \frac{\partial}{\partial t}\left[2mv_0\frac{\partial v}{\partial x}\right] + \frac{\partial}{\partial x}\left[mv_0^2\frac{\partial v}{\partial x}\right] + C_4(x)\frac{\partial v}{\partial t}, \tag{8}$$

$$\frac{\partial}{\partial x}\left[H(x)\frac{\partial u}{\partial x} + EA(x)\left(\frac{\partial u}{\partial x} + \frac{\mathrm{d}y}{\mathrm{d}x}\frac{\partial v}{\partial x}\right)\right] + \frac{\partial^2}{\partial x\,\partial t}\left[C_5(x)\frac{\partial u}{\partial x} + C_6(x)\frac{\partial v}{\partial x}\right] + \frac{C_7(x)}{\omega}\frac{\partial u}{\partial t}$$
$$= \frac{\partial}{\partial t}\left[m(x)\frac{\partial u}{\partial t}\right] + \frac{\partial}{\partial t}\left[2mv_0\frac{\partial u}{\partial x}\right] + \frac{\partial}{\partial x}\left[mv_0^2\frac{\partial u}{\partial x}\right] + C_8(x)\frac{\partial u}{\partial t}. \tag{9}$$

The out-of-plane displacements of the cable are uncoupled from the u and v displacements unless the cable sags under its own weight or carries a spatially nonuniform out-of-plane load [3]. In the present study, it is assumed that the cable carries no out-of-plane load. Consequently, the out-of-plane displacements are excluded from consideration. Also notice that allowance has been made for both viscous and hysteretic damping terms which may be dependent on either velocity or strain rate. The meanings of the damping terms included in the above equations are as follows: $C_1(x)$, $C_2(x)$, $C_5(x)$ and $C_6(x)$ are viscous damping coefficients which are dependent on strain rate components, $C_3(x)$, $C_7(x)$ are hysteretic damping coefficients dependent on velocity components, and $C_4(x)$, $C_8(x)$ are viscous damping coefficients dependent on velocity components. No restriction is placed on damping terms, as their proportion to mass and/or stiffness makes no difference to the ensuing analysis. It may also be noted that the equations allow for cable inhomogenities in mass, stiffness and damping terms. While the above equations remain valid whether or not the cable translates, the ensuing solution is valid for translating cables only if the cable is homogenous. For nontranslating cables, the solutions are more generally valid. The reason for this is that a nonhomogeneous translating cable is a time-varying system, and requires a special solution strategy. This aspect is not considered in this study. Finally, it may be emphasized that the generality with which the damping terms are modeled in this study does not imply that a consistent detailed knowledge of damping mechanisms in cable structures is currently available. Instead, the eventual aim has been applying the formulations developed in this paper to the problem of identification of damping in stranded cable structures.

3
Dynamic stiffness coefficients

When harmonic excitations $P_k(t) = p_k \exp(i\omega t)$ act at the nodes $k = 1, 2, 3$ and 4, of the linear system, all points on the cable oscillate harmonically at the frequency ω. Therefore, one can take $u(x,t) = u(x)\exp(i\omega t)$ and $v(x,t) = v(x)\exp(i\omega t)$ and the equations governing $u(x)$ and $v(x)$ can be shown by

$$\frac{\mathrm{d}}{\mathrm{d}x}\left\{\left[H - mv_0^2 + EA\left(\frac{\mathrm{d}y}{\mathrm{d}x}\right)^2 + i\omega C_2\right]\frac{\mathrm{d}v}{\mathrm{d}x} + \left[EA\frac{\mathrm{d}y}{\mathrm{d}x} + i\omega C_1\right]\frac{\mathrm{d}u}{\mathrm{d}x}\right\} = 2\mathrm{i}\omega m v_0 \frac{\mathrm{d}v}{\mathrm{d}x}$$

$$+\left(-m\omega^2 + \mathrm{i}\omega C_4 + \mathrm{i}C_3\right)v, \tag{10}$$

$$\frac{\mathrm{d}}{\mathrm{d}x}\left\{\left[H - mv_0^2 + EA + \mathrm{i}\omega C_5\right]\frac{\mathrm{d}u}{\mathrm{d}x} + \left[EA\frac{\mathrm{d}y}{\mathrm{d}x} + \mathrm{i}\omega C_6\right]\frac{\mathrm{d}v}{\mathrm{d}x}\right\} = 2\mathrm{i}\omega m v_0 \frac{\mathrm{d}u}{\mathrm{d}x} + (-m\omega^2 + \mathrm{i}\omega C_8 + \mathrm{i}C_7)u. \tag{11}$$

To derive the dynamic stiffness matrix, it is necessary to solve the above pair of equations for two sets of boundary conditions: one on displacements and the other on forces shown, respectively, in Figs. 2 and 3. The boundary conditions on displacements are given by

$$v(0) = \Delta_{R1} + \mathrm{i}\Delta_{I1}; \quad u(0) = \Delta_{R2} + \mathrm{i}\Delta_{I2}; \quad v(L) = \Delta_{R3} + \mathrm{i}\Delta_{I3}; \quad u(L) = \Delta_{R4} + \mathrm{i}\Delta_{I4}; \tag{12}$$

and those on forces are

$$\left[H - mv_0^2 + EA\left(\frac{\mathrm{d}y}{\mathrm{d}x}\right)^2 + \mathrm{i}\omega C_2\right]\frac{\mathrm{d}v}{\mathrm{d}x} + \left[EA\frac{\mathrm{d}y}{\mathrm{d}x} + \mathrm{i}\omega C_1\right]\frac{\mathrm{d}u}{\mathrm{d}x} = p_{R1} + \mathrm{i}p_{I1} \qquad \text{at} \quad x = 0,$$

$$[H - mv_0^2 + EA + \mathrm{i}\omega C_5]\frac{\mathrm{d}u}{\mathrm{d}x} + \left[EA\frac{\mathrm{d}y}{\mathrm{d}x} + \mathrm{i}\omega C_6\right]\frac{\mathrm{d}v}{\mathrm{d}x} = p_{R2} + \mathrm{i}p_{I2} \qquad \text{at} \quad x = 0,$$

$$\left[H - mv_0^2 + EA\left(\frac{\mathrm{d}y}{\mathrm{d}x}\right)^2 + \mathrm{i}\omega C_2\right]\frac{\mathrm{d}v}{\mathrm{d}x} + \left[EA\frac{\mathrm{d}y}{\mathrm{d}x} + \mathrm{i}\omega C_1\right]\frac{\mathrm{d}u}{\mathrm{d}x} = p_{R3} + \mathrm{i}p_{I3} \qquad \text{at} \quad x = L,$$

$$[H - mv_0^2 + EA + \mathrm{i}\omega C_5]\frac{\mathrm{d}u}{\mathrm{d}x} + \left[EA\frac{\mathrm{d}y}{\mathrm{d}x} + \mathrm{i}\omega C_6\right]\frac{\mathrm{d}v}{\mathrm{d}x} = p_{R4} + \mathrm{i}p_{I4} \qquad \text{at} \quad x = L. \tag{13}$$

Notice that $u(x)$ and $v(x)$ become complex in nature due to the presence of damping and axial motion terms. Thus, the above pair of equations constitute a set of complex boundary value problems with nonhomogeneous boundary conditions. These equations can be recast into a set of eight first order equations by introducing the variables $y_k(t)$, $k = 1, 2, \ldots, 8$ through the relations

$$v(x) = y_1(x) + \mathrm{i}y_2(x),$$

$$u(x) = y_3(x) + \mathrm{i}y_4(x),$$

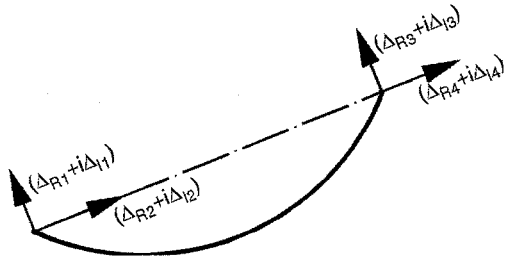

Fig. 2. Displacement boundary conditions

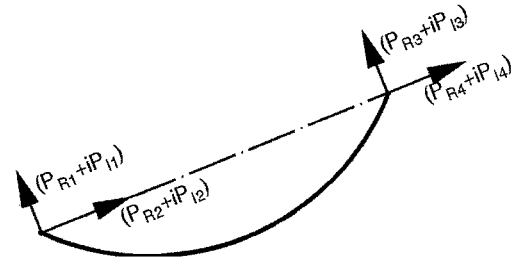

Fig. 3. Force boundary conditions

$$\left[H - mv_0^2 + EA\left(\frac{dy}{dx}\right)^2 + i\omega C_2\right]\frac{dv}{dx} + \left[EA\frac{dy}{dx} + i\omega C_1\right]\frac{du}{dx} = y_5(x) + iy_6(x),$$

$$[H - mv_0^2 + EA + i\omega C_5]\frac{du}{dx} + \left[EA\frac{dy}{dx} + i\omega C_6\right]\frac{dv}{dx} = y_7(x) + iy_8(x). \tag{14}$$

Substituting these equations into (13), and separating real and imaginary parts, one gets

$$\left[H - mv_0^2 + EA\left(\frac{dy}{dx}\right)^2\right]\frac{dy_1}{dx} - \omega C_2\frac{dy_2}{dx} + EA\frac{dy}{dx}\frac{dy_3}{dx} - \omega C_1\frac{dy_4}{dx} - y_5 = 0,$$

$$\omega C_2\frac{dy_1}{dx} + \left[H - mv_0^2 + EA\left(\frac{dy}{dx}\right)^2\right]\frac{dy_2}{dx} + \omega C_2\frac{dy_3}{dx} + EA\frac{dy}{dx}\frac{dy_4}{dx} - y_6 = 0,$$

$$EA\frac{dy}{dx}\frac{dy_1}{dx} - \omega C_6\frac{dy_2}{dx} + [H - mv_0^2 + EA]\frac{dy_3}{dx} - \omega C_5\frac{dy_4}{dx} - y_7 = 0,$$

$$\omega C_6\frac{dy_1}{dx} + EA\frac{dy}{dx}\frac{dy_2}{dx} + \omega C_5\frac{dy_3}{dx} + [H - mv_0^2 + EA]\frac{dy_4}{dx} - y_8 = 0,$$

$$2mv_0\omega\frac{dy_2}{dx} + \frac{dy_5}{dx} + m\omega^2 y_1 + [\omega C_4 - C_3]y_2 = 0,$$

$$-2mv_0\omega\frac{dy_1}{dx} + \frac{dy_6}{dx} + mv_0^2 y_3 + [\omega C_4 - C_3]y_4 = 0,$$

$$2mv_0\omega\frac{dy_4}{dx} + \frac{dy_7}{dx} + m\omega^2 y_3 + [\omega C_8 - C_7]y_4 = 0,$$

$$-2mv_0\omega\frac{dy_3}{dx} + \frac{dy_8}{dx} - [\omega C_8 - C_7]y_3 + m\omega^2 y_4 = 0. \tag{15}$$

These equations constitute a set of simultaneous equations in $\{\mathbf{y}'\}$, and can be recast in the form

$$\mathbf{y}' = \mathbf{A}\mathbf{y}. \tag{16}$$

The prime here denotes the derivative with respect to x. Furthermore, $\mathbf{A}$ is a 8×8 matrix whose elements are functions of x and, consequently, closed form solutions are not in general possible. Analytical techniques may be used to obtain approximate solutions, or, alternatively, resort to numerical methods. Noted again that the governing equations, being boundary value problems, marching techniques, such as the Runge-Kutta algorithms, cannot be directly applied to them. They need to be converted into a set of equivalent initial value problems first.

4
Equivalent set of initial value problems

Consider the matrix of fundamental solutions denoted by $\mathbf{W}$ of Eq. (13) which are obtained by solving (13) under the *initial* conditions

$$W_{ij}(x = 0) = \delta_{ij}, \tag{17}$$

where δ_{ij} is the Kronecker delta function. This would mean that the jth column of the matrix $\mathbf{W}$ consists of solution vector $\mathbf{y}$ (x) of Eq. (16) with initial conditions $y_j(0) = 1$ and $y_i(0) = 0$ for $i \neq j$. Any other solution of $\mathbf{y}(x)$ of Eq. (16) can be written as a linear combination of the elements of $\mathbf{W}$ as

$$\mathbf{y}(x) = \mathbf{W}\boldsymbol{\alpha}, \tag{18}$$

where the vector $\boldsymbol{\alpha}$ needs to be selected to satisfy the prescribed conditions. Thus, for the displacement boundary conditions shown in Fig. 2 one gets

$$\begin{Bmatrix} \Delta_{R1} \\ \Delta_{I1} \\ \Delta_{R2} \\ \Delta_{I2} \\ \Delta_{R3} \\ \Delta_{I3} \\ \Delta_{R4} \\ \Delta_{I4} \end{Bmatrix} = \begin{Bmatrix} 1 & 0 & 0 & 0 & 0 & 0 & 0 & 0 \\ 0 & 1 & 0 & 0 & 0 & 0 & 0 & 0 \\ 0 & 0 & 1 & 0 & 0 & 0 & 0 & 0 \\ 0 & 0 & 0 & 1 & 0 & 0 & 0 & 0 \\ W_{11}(L) & W_{12}(L) & W_{13}(L) & W_{14}(L) & W_{15}(L) & W_{16}(L) & W_{17}(L) & W_{18}(L) \\ W_{21}(L) & W_{22}(L) & W_{23}(L) & W_{24}(L) & W_{25}(L) & W_{26}(L) & W_{27}(L) & W_{28}(L) \\ W_{31}(L) & W_{32}(L) & W_{33}(L) & W_{34}(L) & W_{35}(L) & W_{36}(L) & W_{37}(L) & W_{38}(L) \\ W_{41}(L) & W_{42}(L) & W_{43}(L) & W_{44}(L) & W_{45}(L) & W_{46}(L) & W_{47}(L) & W_{48}(L) \end{Bmatrix} \begin{Bmatrix} \alpha_1 \\ \alpha_2 \\ \alpha_3 \\ \alpha_4 \\ \alpha_5 \\ \alpha_6 \\ \alpha_7 \\ \alpha_8 \end{Bmatrix}, \quad (19)$$

which can be written concisely as

$$\boldsymbol{\Delta} = \mathbf{S}_1 \boldsymbol{\alpha}. \quad (20)$$

Similarly, from the boundary forces shown in Fig. 3 one gets

$$\begin{Bmatrix} p_{R1} \\ p_{I1} \\ p_{R2} \\ p_{I2} \\ p_{R3} \\ p_{I3} \\ p_{R4} \\ p_{I4} \end{Bmatrix} = \begin{Bmatrix} 0 & 0 & 0 & 0 & 1 & 0 & 0 & 0 \\ 0 & 0 & 0 & 0 & 0 & 1 & 0 & 0 \\ 0 & 0 & 0 & 0 & 0 & 0 & 1 & 0 \\ 0 & 0 & 0 & 0 & 0 & 0 & 0 & 1 \\ W_{51}(L) & W_{52}(L) & W_{53}(L) & W_{54}(L) & W_{55}(L) & W_{56}(L) & W_{57}(L) & W_{58}(L) \\ W_{61}(L) & W_{62}(L) & W_{63}(L) & W_{64}(L) & W_{65}(L) & W_{66}(L) & W_{67}(L) & W_{68}(L) \\ W_{71}(L) & W_{72}(L) & W_{73}(L) & W_{74}(L) & W_{75}(L) & W_{76}(L) & W_{77}(L) & W_{78}(L) \\ W_{81}(L) & W_{82}(L) & W_{83}(L) & W_{84}(L) & W_{85}(L) & W_{86}(L) & W_{87}(L) & W_{88}(L) \end{Bmatrix} \begin{Bmatrix} \alpha_1 \\ \alpha_2 \\ \alpha_3 \\ \alpha_4 \\ \alpha_5 \\ \alpha_6 \\ \alpha_7 \\ \alpha_8 \end{Bmatrix}, \quad (21)$$

which, again, can be written compactly as

$$\mathbf{P} = \mathbf{S}_2 \boldsymbol{\alpha}. \quad (22)$$

It follows from Eqs. (20) and (22) that

$$\mathbf{P} = \mathbf{S}_2 \mathbf{S}_1^{-1} \boldsymbol{\Delta} = \mathbf{D} \boldsymbol{\Delta}, \quad (23)$$

where $\mathbf{D} = \mathbf{S}_2 \mathbf{S}_1^{-1}$ can be interpreted as the modified dynamic stiffness matrix which takes into account the complex nature of stiffness coefficients arising from the presence of damping and Coriolis terms due to axial motion.

5
Particular integral

In the dynamic stiffness formulations for built-up structures, the nodes can be taken to be located at support points and at intersections of different structural elements. If excitation forces are applied at the nodes of cable element, as in the case of seismic excitations transmitted through the cable supports, the dynamic stiffness matrix can be used directly in formulating the equilibrium conditions, and, subsequently, in the determination of the response. On the other hand, if excitations are applied at points other than nodes, as in the case of wind loads, the dynamic stiffness matrix needs to be modified. This can be realized by considering an additional particular integral to the solution already obtained for time-varying support conditions. To illustrate this, consider a cable element carrying a concentrated harmonic load at a point x_0 as shown in Fig. 1. To write down the particular integral we first find the solution of Eq. (16) with initial conditions $y(0)^* = [0, 0, 0, 0, 1, 0, 0, 0]$, here * denotes matrix transposition. This defines the impulse response function with which we convolve the external forcing to obtain the desired solution. The function has already been determined $y_5(x)$, that is, the fifth column of the matrix $\mathbf{W}$. Consequently, the total solution can be written as

$$\begin{cases} \mathbf{y}(x) = \mathbf{W}(x)\alpha & \text{for} \quad x \leqq x_0, \\ \mathbf{W}(x)\alpha + Q \int_{x_0}^{x} y_5(x-\tau)\delta(\tau - x_0)\,\mathrm{d}\tau & \text{for} \quad x \geqq x_0. \end{cases} \quad (24)$$

Following the arguments used in deriving Eq. (23), it is shown that the nodal forces and displacements are related through the relation

$$\mathbf{P} = \mathbf{D}(\boldsymbol{\Delta} - \boldsymbol{\Delta}_a) + \boldsymbol{\Delta}_b, \tag{25}$$

where

$$\boldsymbol{\Delta}_a^* = \{0, 0, 0, 0, QW_{55}(L - x_0), \quad QW_{65}(L - x_0), \quad QW_{75}(L - x_0), \quad QW_{85}(L - x_0)\}$$

$$\boldsymbol{\Delta}_b^* = \{0, 0, 0, 0, QW_{15}(L - x_0), \quad QW_{25}(L - x_0), \quad QW_{35}(L - x_0), \quad QW_{45}(L - x_0)\}. \tag{26}$$

This formulation can be easily generalized to include the effects of distributed loads and forces in the other directions. For the case of distributed loads, the convolution with system impulse response will have to be evaluated numerically.

6
Numerical results

A computer program based on the formulation presented in the preceding sections has been developed. The matrix of fundamental solutions W has been generated by using a fourth-order Runge-Kutta method. Thus, to generate the dynamic stiffness coefficients for one value of frequency ω, the set of equations given in (16) were integrated with eight independent sets of initial conditions. For the frequency range surveyed, an integration step size of $L/1000$ was found to give satisfactory results. By way of validating the program developed, the following qualitative and quantitative checks have been made:

- Matching of natural frequencies obtained using this program with values reported in literature for cables of different spans.
- Satisfaction of reciprocity requirements of the system's Green function and symmetry properties of dynamic stiffness coefficients.
- Approach to the exactly known limits on dynamics stiffness coefficients and the Green functions as cable span goes to zero and the system behaves as a string.
- Display of the well-known qualitative features of resonances, anti-resonances and minima of direct and cross receptance functions.

Figure 4 shows the modulus of $\Delta_{R1} + i\Delta_{I1}$ for a cable with $L = 100$ m, $A = 5.79 \times 10^{-4}$ m^2, $E = 20.684 \times 10^{10}$ N/m^2, $H_0 = 29403$ N, $m = 2.2$ kg/m and $\theta = 30°$, which is taken to translate at an uniform velocity of 30 m/s. The results are shown for two damping models: firstly, a velocity-dependent viscous damping model with $C_4 = C_8 = 0.66$ Ns/m^2 and with all other damping coefficients C_k being zero. Secondly, a strain-rate-dependent viscous damping model with $C_2 = C_6 = 20$ Ns and other C_k being zero. The choice of the damping coefficients is based on the criterion that the modal damping coefficients in the first mode in both cases is about 5%. In the first case, the modal band-width remains

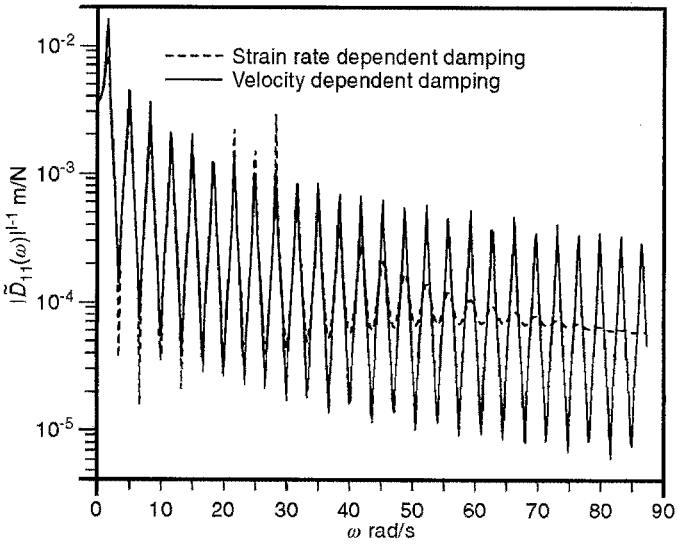

Fig. 4. Magnitude of stiffness coefficient; $L = 100$ m, $A = 9.734 \times 10^{-4}$ m^2, $E = 20.684 \times 10^{10}$N/m^2, $H_0 = 29403$ N and $\theta = 30°$

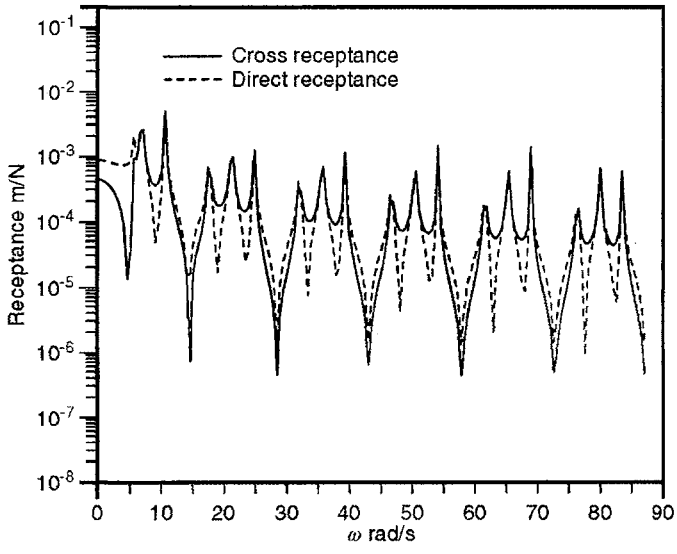

Fig. 5. Direct and cross-receptance functions; $L = 100$ m, $A = 9.734 \times 10^{-4}$ m^2, $E = 20.684 \times 10^{10}$ N/m^2, $H_0 = 29403$ N, $v_0 = 0$ and $\theta = 0°$

constant for all modes, while for the second it increases with increases in frequency. Consequently, the two transfer functions show qualitatively different behavior in higher-frequency regions. This feature is of significant interest in high-frequency vibration analysis using statistical models for the vibrating systems [5]. The Green function moduli for the same cable with $\theta = 0°$ and $v_0 = 0$ under the action of a harmonic excitation at $x_0 = 25$ m for response measured at $x = 25$ m and 75 m using the particular integral derived in Eqs. (24) and (25) are shown in Fig. 5. For the case of drive point and measurement point being identical, the resonant and the anti-resonant peaks are observed to alternate, which is consistent with well-known features of the direct receptance functions. Conversely, for the cross-receptance, that is, for $x_0 = 25$ m and $x = 75$ m, between successive resonant peaks one gets either a minimum or an anti-resonant peak. This is consistent with the known properties of these functions.

7
Random vibration analysis of multi-support earthquake response

The usefulness of formulations developed in Sects. 3–5 is not necessarily restricted to harmonic response analysis. In conjunction with the Laplace or Fourier transform techniques, they can be used for transient vibration analysis also. Similarly, the results can be used directly in stationary random vibration analysis in frequency domain, in which case, the stiffness coefficients serve as the system transfer functions and enable the spectral analysis in an elegant fashion. To illustrate this, the response of a 1000-m-long cable which is fixed at the two ends and supported at the same level is considered. The two supports are taken to be acted upon by stationary vector random excitations with power spectral density (PSD) functions of support accelerations $\ddot{f}_1(t)$ and $\ddot{f}_2(t)$ given by

$$S_{\ddot{f}_1\ddot{f}_1}(\omega) = S_{\ddot{f}_2\ddot{f}_2}(\omega) = \frac{\phi_0\left[1 + 4\zeta_g\left(\frac{\omega}{\omega_g}\right)^2\right] \qquad \left(\frac{\omega}{\omega_f}\right)^4}{\left[1 - \left(\frac{\omega}{\omega_g}\right)^2\right]^2 + 4\zeta_g\left(\frac{\omega}{\omega_g}\right)^2\left[1 - \left(\frac{\omega}{\omega_f}\right)^2\right]^2 + 4\zeta_f\left(\frac{\omega}{\omega_f}\right)^2}, \tag{27}$$

$$S_{\ddot{f}_1\ddot{f}_2}(\omega) = S_{\ddot{f}_1\ddot{f}_2}(\omega)\exp\left[-\left(\frac{\gamma L\,\omega}{V}\right)^2 + i\omega\tau\right]. \tag{28}$$

The free vibration of this cable has been studied earlier in [9]. For nondimensional cable parameters $\Gamma = EA/H = 256.75$ and $\beta = mgL/H = 0.72$, the first few natural frequencies in the predominantly vertical modes have been reported to be 0.11, 0.16, 0.20, 0.23, 0.30 and 0.35 Hz. Those in the predominantly longitudinal modes are 0.99, 1.93, 2.88, 3.83, 4.79 and 5.74 Hz. In the present study, we take $E = 8.75 \times 10^{10}$ N/m^2, $A = 9.62 \times 10^{-4}$ m^2, $mg = 236.04$ N/m, and $H_0 = 327837.0$ N which correspond to $\Gamma = 256.75$ and $\beta = 0.72$. The damping is assumed to be viscous with $C_4 = C_8 = 0.2$ Ns/m^2 with all other C_k being zero. The model for the seismic excitation is taken from [17]. As seen in Eq. (27), the PSD function $S_{\ddot{f}_1\ddot{f}_1}(\omega)$ has two parts: first, the well-known Kanai-Tajimi spectrum which models the filtering action of the soil layer, and second, a singularity-suppressing filter which makes

the ground displacements well behaved [1]. In the numerical work, it is assumed that the dominant ground frequency $\omega_g = 5.0\,\pi$ rad/s, soil damping $\eta_g = 0.6$, intensity $\phi_0 = 1.0\ \mathrm{m^2/s^3}$. $\gamma = 0.4$, transmission time lag $\tau = 1$ s, wave velocity $V = 1000.0$ m/s, filter frequency $w_f = 5.5$ rad/s and filter damping $\zeta_f = 0.53$.

In our study, we assume that the support accelerations $\ddot{f}_1(t)$ and $\ddot{f}_2(t)$ act along the directions 1 and 3, see Fig. 1, and compute the PSD function of the horizontal and vertical forces transmitted to the left end support in terms of the dynamic stiffness coefficients determined using the procedure outlined in Sects. 3–5. Thus, it is possible to show that the PSD of the force transmitted vertically to the left support is given by

$$S_v(\omega) = H_1(\omega) S_{f_1,f_1}(\omega) + H_2(\omega) S_{f_2,f_2}(\omega) + 2\mathrm{Re}\{H_3(\omega) S_{f_1,f_2}(\omega)\}, \tag{29}$$

where

$$H_1(\omega) = [D_{11}(\omega)^2 + D_{12}(\omega)^2],$$

$$H_2(\omega) = [D_{15}(\omega)^2 + D_{16}(\omega)^2], \tag{30}$$

$$H_3(\omega) = [D_{11}(\omega) - \mathrm{i}D_{12}(\omega)]\,[D_{15}(\omega) + \mathrm{i}D_{16}(\omega)].$$

Similarly, the PSD of horizontal force transmitted to left support can be shown to be given by

$$S_h(\omega) = H_4(\omega) S_{f_1,f_1}(\omega) + H_5(\omega) S_{f_2,f_2}(\omega) + 2\mathrm{Re}\,[H_6(\omega) S_{f_1,f_2}(\omega)], \tag{31}$$

where

$$H_4(\omega) = [D_{31}(\omega)^2 + D_{32}(\omega)^2],$$

$$H_5(\omega) = [D_{35}(\omega)^2 + D_{36}(\omega)^2], \tag{32}$$

$$H_6(\omega) = [D_{31}(\omega) - \mathrm{i}D_{32}(\omega)]\,[D_{35}(\omega) + \mathrm{i}D_{36}(\omega)].$$

The variations of $H_1(\omega)$ and $H_4(\omega)$ are shown in Figs. 6 and 7 respectively. The response PSD functions $S_v(\omega)$ and $S_h(\omega)$ are plotted in Figs. 8 and 9 respectively. The coupling between transverse and longitudinal modes of vibration is clearly evident in Figs. 6 and 7. The transverse response in Fig. 6 displays packing of peaks due to predominantly longitudinal modes with more densely spaced transverse vibration resonances. Conversely, in Fig. 7, as might be reasonably expected, the response is dominated by longitudinal modes, the effect of transverse vibrations still being felt through perturbations in the vicinity of antiresonance points. These features are again to be seen in Figs. 8 and 9, wherein the transverse reaction receives contributions from both transverse and longitudinal modes, while the horizontal reactions are dominated by longitudinal modes. It has been verified for

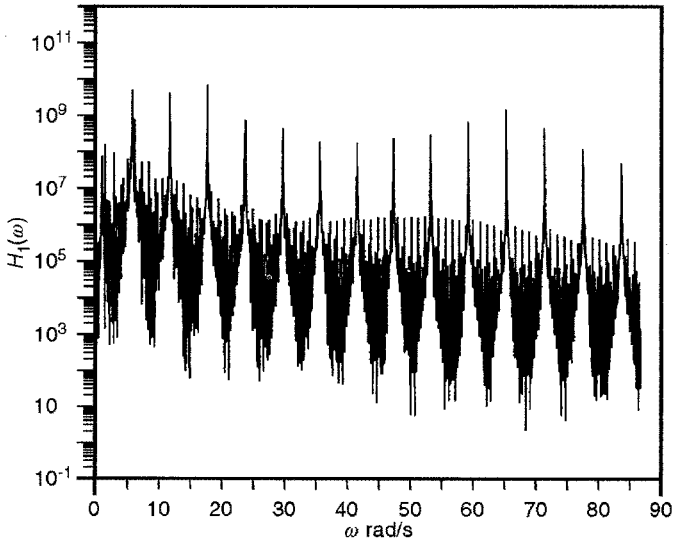

Fig. 6. Transfer function H_1 for the 1000 m cable

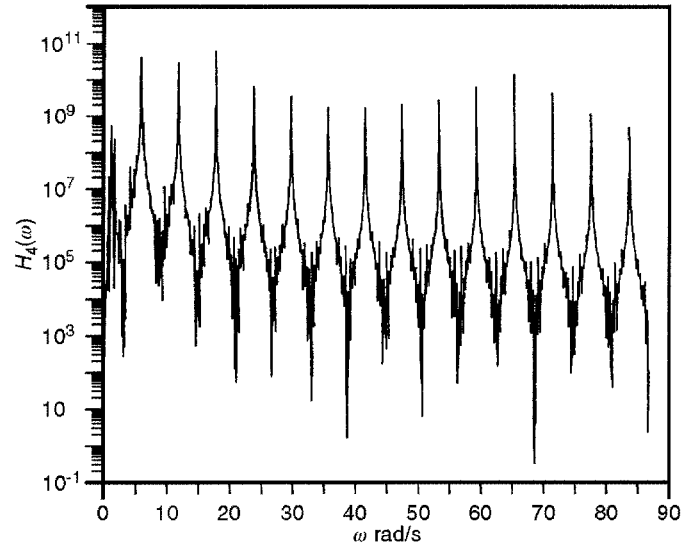

Fig. 7. Transfer function H_4 for the 1000 m cable

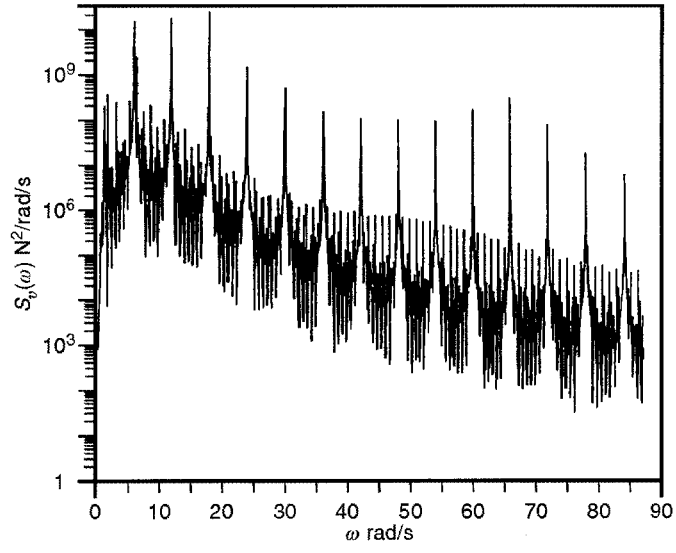

Fig. 8. PSD of the vertical force transmitted to the left support

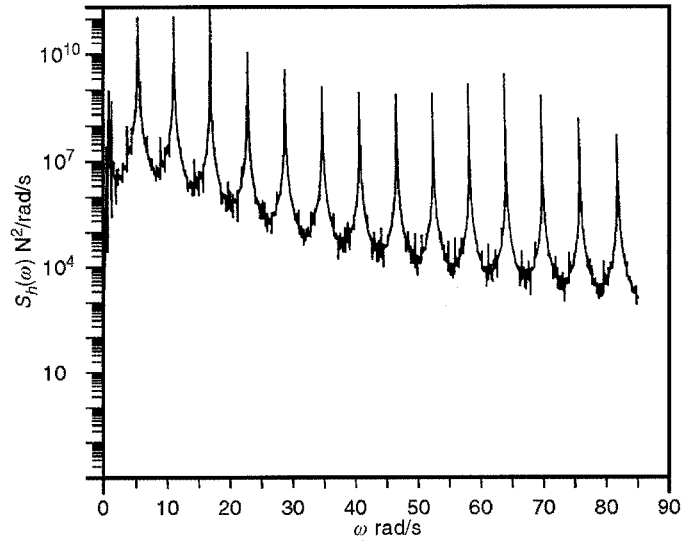

Fig. 9. PSD of the horizontal force transmitted to the left support

the first few peaks in Figs. 6 and 7, that their location is in agreement with the natural frequencies as reported in [9] for the same cable.

It may be pointed out in this context that earthquake inputs can be specified through PSD functions or through a set of response spectra as is more popularly done. Here, it must be noted that the dynamic stiffness matrix formulation, as developed in this paper, does not provide information on the cable free vibration characteristics, such as mode shapes and natural frequencies. It may be still possible to infer them easily, at least the natural frequencies, by studying the location of peaks in the undamped stiffness coefficient spectrum. This can make difficult the application of the technique to seismic response analysis problems when the earthquake inputs are specified through a set of response spectra. This is because the response spectra are primarily defined for single degree of freedom systems. When used for analyzing multi-degree freedom systems, the method involves summing modal maximum responses using empirical relations [1]. This difficulty can easily be circumvented if a PSD function compatible with the given response spectra is obtained, in which case, the dynamic stiffness coefficients enable the subsequent response analysis. Such an approach, in fact, is more appropriate when considering systems with densely packed modes such as the 1000-m cable studied in this paper, for which the results of empirical summation procedures can be unreliable.

8
Conclusions

A numerical scheme for the study of harmonic response analysis of a fairly general cable element is outlined. The effects of coupling between inplane and transverse motions, inclined cable supports, axial translation, proportional/nonproportional and viscous/hysteretic damping models, multi-support motions, arbitrary loads within the cable span, and inhomogenities in cable inertia and stiffness for non-translating cables are included in the analysis. The application of the proposed scheme to the seismic response analysis of a long span cable with multiple-support random excitations is demonstrated. The assumption of small sag-to-span ratio and the consequent treatment of $ds \simeq dx$ is not crucial: the method can be generalized within the framework of linear dynamics to treat s as the independent variable, in which case, large sag cables can also be studied. Further extensions to the study of built-up structures, such as multi-span and multiple cable systems as used in power transmission lines, is also possible. A damping identification scheme for suspended cable structures is currently being developed by the present authors based on the procedure outlined in this paper.

References

1. **Clough, R. W.; Penzien, J.:** Dynamics of structures. Tokyo: McGraw-Hill Kogakusha 1992
2. **Irvine, M.:** Cable structures. New York: Dover Publications 1981
3. **Iyengar, R. N.; Rao, G. V.:** Free vibrations and parametric instability of a laterally loaded cable. J. Sound Vib. 127 (1988) 231–243
4. **Lee, S. Y.; Kuo, Y. H.:** Exact solutions for the analysis of general elastically restrained nonuniform beams. Trans. ASME/J. Appl. Mech. 59 (1992) 205–212
5. **Manohar, C. S.; Keane, A. J.:** Statistics of energy flows in spring coupled one dimensional subsystems. Phil. Trans. R. Soc. Lond. A 346 (1994) 525–542
6. **Migliore, H.; Webster, R. L.:** Current methods for analyzing cable response 1979 to the present. Shock Vib. Dig. 14 (1982) 19–24
7. **Paz, M.:** Structural dynamics. New Delhi: CBS Publishers 1985
8. **Rao, G. V.:** Vibration of cables under deterministic and random excitations. PhD thesis, Department of civil engineering, Indian Institute of Science, 1989
9. **Rao, G. V.; Iyengar, R. N.:** Seismic response of a long span cable. Earthquake Eng. Struct. Dyn. 20 (1991) 243–258
10. **Starossek, U.:** Dynamic stiffness matrix of sagging cable. J. Eng. Mech. 117 (1991) 2815–2829
11. **Triantfyllou, M. S.:** Dynamics of cables, towing cables and mooring systems. Shock Vib. Dig. 23 (1991) 3–8
12. **Velestos, A. S.; Darbre, G. R.:** Dynamic stiffness of parabolic cables. Earthquake Eng. Struct. Dyn. 11 (1983) 367–401
13. **Vinogradov, O. G.; Pivovarov, I.:** The phenomenon of damping in stranded cables. In: Proc. 26th SDM Conf., Orlando, Florida, USA, 1985 pp. 232–237 AIAA
14. **Wickert, J. A.; Mote, C. D. Jr.:** Current research on the vibration and stability of axially moving materials. Shock Vib. Dig. 20 (1988) 3–13
15. **Yang, B.:** Transfer functions of constrained/combined one-dimensional continuous dynamic systems. J. Sound Vib. 156 (1992) 425–443
16. **Yang, B.:** Distributed transfer function analysis of complex distributed parameter systems. Trans. ASME Appl. Mech. 61 (1994) 84–92
17. **Zerva, A.:** Effect of spatial variability and propagation of seismic ground motions on the response of multiply supported structures. Probabilistic Eng. Mech. 6 (1991) 212–221